PFC/JA-89-16

Measurement of Suprathermal Electrons in Tokamaks Via Electron Cyclotron Transmission

R.K. Kirkwood, I.H. Hutchinson,
S.C. Luckhardt and J.P. Squire

March 1990

Plasma Fusion Center
and
Research Laboratory of Electronics

Massachusetts Institute of Technology
Cambridge, Massachusetts 02139 USA

Measurement of Suprathermal Electrons in Tokamaks Via Electron Cyclotron Transmission

R. K. Kirkwood, I. H. Hutchinson, S. C. Luckhardt, and J. P. Squire

Plasma Fusion Center and Research Laboratory of Electronics

Massachusetts Institute of Technology

Cambridge, Massachusetts, U. S. A.

Abstract

The momentum distribution of the current carrying suprathermal electrons is determined from the measurement of X mode transmission near the fundamental of the cyclotron frequency during inductive and radio frequency current drive in the Versator II tokamak. The measurement of the differential attenuation of radiation of two beams with finite and opposite $N_{||}$ allows the separation of the wave attenuation due to cyclotron absorption from that due to non–resonant mechanisms. It is shown that such transmission measurements can be used to determine the part of the parallel momentum distribution, which is asymmetric in $p_{||}$, $F_a(p_{||}) \equiv \frac{1}{2}(F(-p_{||}) - F(p_{||}))$. Measurements of $F(p_{||})$ and its time evolution generally agree with expectations, although $T_{||}$ is found to be lower than predicted by collisional theory in the inductively driven case.

Introduction

The interaction of energetic electrons with electromagnetic radiation near the cyclotron harmonic frequency in tokamaks is of wide interest for heating [1,2] and current generation [2,3,4], as well as for diagnosing electron distributions [5,6,7]. Previous authors [7] have demonstrated absorption of normally incident radiation on relativistic electrons at frequencies just below the cyclotron frequency. In this paper the electron cyclotron absorption mechanism is investigated both theoretically and experimentally for radiation oblique to the magnetic field in a tokamak. It is found that measurements of the frequency dependent absorption provide a measure of the momentum distribution of the energetic electron population. In particular, we have chosen to launch waves with a non–zero value of the parallel index of refraction ($N_{||}$) in a plasma where the current is carried by weakly relativistic electrons. In this case we find a nearly one to one correspondence between the absorption at a particular frequency and the perpendicularly averaged distribution function $F(p_{||})$ ($\equiv 2\pi \int_0^\infty p_\perp f(p_\perp,p_{||})\, dp_\perp$) at a particular $p_{||}$ as well as an independent measure of the refractive effects on the transmitted ray amplitude. Experiments have been performed on the Versator II tokamak to measure the momentum distribution of the energetic electron population that carries the current in low density inductive discharges and in Lower Hybrid Current Driven (LHCD) discharges. Section II reviews the theory of electron cyclotron absorption and refraction at frequencies below the electron cyclotron frequency, ω_{ce}, and develops the method for measuring $F(p_{||})$. Section III describes the experimental apparatus. Section IV presents the experimental results for refraction, absorption, and electron momentum distributions and compares them with theory and with other fast particle measurements. Conclusions are presented in Section V.

II. Theory of Wave Absorption Near $\omega = \omega_{ce}$

In order to understand the absorption of waves near $\omega_{ce}/\omega = 1$, first consider the relativistic electron wave resonance condition [8]

$$\gamma - \omega_{ce}/\omega - N_{||}p_{||} = 0 \qquad (1$$

Where γ is the relativistic factor $\gamma = (1 + p^2)^{1/2}$, $N_{||}$ is the parallel index of refraction, $p_{||}$ is the component of momentum parallel to B in units of mc, and ω_{ce} and ω are the cyclotron and wave frequencies respectively. This condition defines a relationship between $p_{||}$, $p_{\perp}$, $N_{||}$, and ω necessary for wave–particle interaction. Figure 1 shows the elliptical contours in $\bar{p}$ space along which the resonance condition is satisfied for various wave $N_{||}$ and ω. The spatial damping rate of the wave will be determined by the integral of the derivatives of the momentum distribution function over these contours. To use cyclotron absorption measurements for diagnosing distribution functions it is important to choose the wave parameters such that the required information about $f(\bar{p})$ is most easily extracted from the measured data (usually the absorption rate averaged along a ray path). The choice of the resonance contour with $\omega_{ce}/\omega \geq 1$ and $N_{||}$ finite (oblique propagation) allows measurement of the parallel distribution function $F(p_{||})$. The advantage of finite $N_{||}$ is that the contours are shifted ellipses such that there is only one intersection of the $p_{||}$ axis at a sufficiently low energy to interact with particles (here assumed to have energies E < 200 keV). This allows the wave to interact with particles of a particular value of $p_{||}$ for a distribution where $T_{\perp}$ is sufficiently small. The advantage of $\omega_{ce}/\omega \geq 1$ is that the ellipses extend to large $T_{\perp}$ and are far from the $p_{||}$ axis so that the upper limit placed on $T_{\perp}$ to insure interaction at a single value of $p_{||}$ is relatively large. For the choice of $N_{||}$ = 0.4 and $1 \leq \omega_{ce}/\omega$ the requirement for a nearly single valued $p_{||}$ interaction is E ≤ 200 keV, $T_{\perp} \lesssim 15$ keV. These requirements are well–suited to the small fraction of energetic current carrying electrons produced during Ohmic slide away or lower hybrid current drive (LHCD) plasmas in Versator II and will be assumed to be satisfied for the purpose of theoretical analysis. The validity of these assumptions will be discussed for the particular experimental conditions in section IV. In these experiments the resonant contour is held nearly constant along a ray path by maintaining $N_{||}$ and

ω_{ce}/ω constant. In the tokamak geometry this is achieved with a vertical ray path tangential to the surface of constant major radius R. The distribution function is related to the absorption rate along such a ray path by a calculation following Ref. [8].

Cyclotron absorption is calculated from the dispersion tensor [8] expanded to lowest order in $k_\perp \rho_e$ (valid for $T_\perp \leq 15$ keV). In these experiments the plasma consists of two populations of electrons, a very low temperature bulk, and a very small population of suprathermal electrons. The real parts of the dispersion relation, D, are dominated by the bulk plasma and give the usual cold plasma dispersion relation, while the imaginary parts of D are dominated by the resonant interaction with the suprathermal particles provided $|k_\parallel v_e| << |\omega - \omega_{ce}|$ where v_e is the bulk thermal velocity. In this limit, the anti–Hermitian parts of the dielectric tensor ε''_{11}, ε''_{13}, ε''_{33}, are given by

$$\varepsilon''_{ij} \simeq -\frac{\pi^2 \omega_p^2}{2\omega^2} \int_{p_-}^{p_+} \left[\frac{N_\perp p_\parallel \omega}{\omega_{ce}}\right]^{n_{i,j}} p_\perp \left[\frac{\omega_c}{\omega}\frac{\partial}{\partial p_\perp} + N_\parallel p_\perp \frac{\partial}{\partial p_\parallel}\right] f(p_\perp, p_\parallel)\Big|_{p_{\perp o}} dp_\parallel \qquad (2$$

$$p_{\perp o} = ((N_\parallel p_\parallel + \omega_{ce}/\omega)^2 - 1 - p_\parallel^2)^{1/2}$$

$$n_{i,j} = \delta_{i,3} + \delta_{j,3}$$

$$p_\pm = (N_\parallel \omega_{ce}/\omega \pm (\omega_{ce}^2/\omega^2 - 1 + N_\parallel^2)^{1/2})/(1 - N_\parallel^2)$$

which corresponds to Eq. 8 of Ref [8] with $\varepsilon''_{22} = \varepsilon''_{11}$, $i\varepsilon''_{12} = \varepsilon''_{11}$, and $\varepsilon''_{23} = i\varepsilon''_{13}$. The integration follows the resonance contour shown in figure 1.

With the following approximations: $|d(\ln(F(p_\parallel)))/d\, p_\parallel| \lesssim 1/p_\parallel$, $p_\perp << (p_\parallel)^{1/2}$, and $p_\parallel \leq 1$, and $N_\parallel \simeq .4$ which are reasonable for slide away and RF driven distributions, the integral in Eq. 2 can be done by parts to obtain

$$\varepsilon''_{ij} \simeq G_{ij}(\omega_p/\omega, \omega_{ce}/\omega, N_\parallel) \cdot F(p_{\parallel o}) \qquad (3$$

$$p_{\parallel o} = (N_\parallel \omega_{ce}/\omega - N_\parallel/|N_\parallel|\ (\omega_{ce}^2/\omega^2 - 1 + N_\parallel^2)^{1/2})/(1 - N_\parallel^2)$$

$$G_{ij} = \frac{\pi \omega_p^2 \omega_{ce}}{2\omega^3} \frac{N_\parallel}{|N_\parallel|} [p_{\parallel o}(N_\parallel^2 - 1) + N_\parallel \omega_{ce}/\omega]^{-1} [N_\perp p_{\parallel o} \omega/\omega_{ce}]^{n_{i,j}}$$

From Eq. 3 it is evident that all anti–Hermitian parts of ε_{ij} are proportional to a function of cold plasma factors and the resonant momentum $p_{\|o}$, and the quantity of interest $F(p_{\|o})$.

The imaginary part of k is then calculated from the imaginary part of the plasma dispersion relation D which is expanded for $k_i << k_r$ to give

$$\frac{c}{\omega}\bar{k}_i\cdot\hat{v}_g = -\,\mathrm{Imag}(D)\,/\,((\partial D_c/\partial N_{\|})^2+(\partial D_c/\partial N_{\perp})^2)^{1/2} \qquad (4$$

where $\hat{v}_g$ is a unit vector in the direction of the group velocity. D_c is the cold plasma dispersion relation given by

$$\begin{aligned} D_c = {} & \varepsilon_{c1}N_{\perp}^4 + [(\varepsilon_{c1}+\varepsilon_{c3})N_{\|}^2 - \varepsilon_{c1}\varepsilon_{c3} - (\varepsilon_{c1}^2-\varepsilon_{c2}^2)]N_{\perp}^2 \\ & + \varepsilon_{c3}N_{\|}^4 - 2\varepsilon_{c1}\varepsilon_{c3}N_{\|}^2 + \varepsilon_{c3}(\varepsilon_{c1}^2-\varepsilon_{c2}^2) \qquad (5 \\ & \varepsilon_{c1} = 1-\frac{X}{(1-Y^2)},\ \varepsilon_{c2} = \frac{XY}{(1-Y^2)},\ \varepsilon_{c3} = (1-X) \\ & X = \omega_{pe}^2/\omega^2,\ Y = \omega_{ce}/\omega \end{aligned}$$

The imaginary part of D, D_i is given by

$$\begin{aligned} D_i = {} & \varepsilon''_{11}\,[2(\varepsilon_{c1}-N_{\|}^2)(\varepsilon_{c3}-N_{\perp}^2) - N_{\perp}^2(\varepsilon_{c3}-N_{\perp}^2) - N_{\perp}^2N_{\|}^2 - 2\varepsilon_{c2}(\varepsilon_{c3}-N_{\perp}^2)] \\ & + \varepsilon''_{13}\,[-2(\varepsilon_{c1}-N^2)N_{\perp}N_{\|} - 2\varepsilon_{c2}N_{\perp}N_{\|}] \qquad (6 \\ & + \varepsilon''_{33}\,[(\varepsilon_{c1}-N_{\|}^2)^2 - N_{\perp}^2(\varepsilon_{c1}-N_{\|}^2) - \varepsilon_{c2}^2] \end{aligned}$$

so that Eq. 3–6 give a relation between k_i and $F(p_{\|})$.

$$\frac{c}{\omega}k_i\cdot\hat{v}_g = I(\omega_p/\omega,\ \omega_{ce}/\omega,\ N_{\|})\,F(p_{\|o}) \qquad (7$$

under the conditions stated above. Eq. 7 demonstrates that the damping rate of radiation propagating oblique to the magnetic field can provide a direct measure of the parallel distribution function at a particular $p_{\|}$ and a known function of cold plasma parameters. The value of $p_{\|o}$ is determined by Eq. 3 and can be adjusted by selection of the launched wave frequency. Together these relations provide the theoretical basis for a measurement of the distribution of suprathermal electrons as a function of their parallel momentum. The calculations are generalizations of work done for the more restrictive cases of $N_{\|} = 0$ [9] and $F(p_{\|})$ equal to a constant [10].

These results are in agreement with numerical calculations of the imaginary part of N ($N_i = ck_i/\omega$)

where the density of suprathermal particles is taken as independent of $p_{||}$ and Maxwellian in $p_{\perp}$. This calculation is shown in figure 2 for the above case where radiation is launched in the X mode in a plasma with Versator parameters, parabolic density profiles for both bulk and suprathermal particles, and the perpendicular temperature of the suprathermals is 1 keV. N_i is averaged over a straight ray path tangential to the cylindrical surface of constant R, assuming $B_\varphi >> B_R$ or B_Z. This particular geometry forces $N_{||}$, ω_{ce}/ω, and the resonance contour to be nearly constant along the ray path.

There are, however, processes aside from cyclotron absorption which affect the transmitted wave amplitude and the determination of the distribution function from attenuation measurements. The primary one is refraction, which leads to bending of the straight ray paths and to the focusing and defocusing of wave power. This affects the power at the receiving horn. Ray bending can also cause a variation of ω_{ce}/ω along the ray path, since in the tokamak geometry $B_\varphi \cong B_{\varphi o}R_o/R$ a ray that bends out of a path along constant R will sample various ω_{ce}/ω along its path. Ray bending can also lead to a variation of $N_{||}$ along the ray path, both because k_φ is proportional to 1/R and because of poloidal field effects. The variation of ω_{ce} and $N_{||}$ have been investigated using the fully toroidal ray tracing code TORCH [11] which shows that for vertically incident X–mode radiation these quantities are nearly constant along a ray path ($\Delta\omega_{ce}/\omega \leq 8\%$, $\Delta N_{||}/N_{||} \leq 5\%$). For the rays of interest, in a transmission measurement where the transmitting and receiving points are fixed, plasma refraction leads to values of $N_{||}$ as much as 30% greater than in vacuum. The latter effect is dependent on the plasma parameters and can be calculated for each case of interest to provide the correct value of $N_{||}$ in the formulas for $F(p_{||})$.

The most important effect of refraction is found to be the reduction of wave amplitude caused by plasma refraction. Plasma refraction causes the wave amplitude at the receiving horn to be lower than it would be in vacuum through two mechanisms. First the wave amplitude is affected by the change in the divergence of the ray paths (defocusing) which results a broadening of the launched antenna pattern and a reduction of the received power density. Second, ray bending causes a change in the

angles of transmission and reception of the ray path connecting the transmitter and receiver. This leads to a change in the ray amplitude if the source and receiver have radiation patterns that are dependent on angle. These effects are calculated by using the TORCH code to follow a bundle of rays that surround the ray which intersects the receiver. The divergence and launch angle of these rays is then combined with the measured antenna patterns of the launching and receiving horns to obtain the reduction of received power due to plasma refraction. The ray amplitude is found to be reduced by as much as 70% in the Versator case, with the greatest reduction near $\omega_{ce}/\omega = 1$. Compensating for these effects in experimental data by numerical calculation would require a detailed knowledge of the plasma density profile, as well as antenna patterns.

In this work, instead of relying on a calculation of the non–resonant attenuation effects, the asymmetry of the electron distribution in $p_{||}$ is exploited to allow a direct measure of them. This can be understood by examining the resonance condition, Eq. 1, when the sign of $N_{||}$ is changed. Changing the sign of $N_{||}$ rotates the resonance contours by π about the $p_{\perp}$ axis mapping $p_{||}$ to $-p_{||}$. The ratio of transmitted power with $\pm$ values of $N_{||}$ can then be related to the difference in absorption rates and hence the difference

$$F(-p_{||o}) - F(p_{||o}) \simeq \frac{c}{\omega} I(\omega_{ce}/\omega, \omega_p/\omega, N_{||})^{-1} \left(\text{Imag}(k)\big|_{N_{||}=+} - \text{Imag}(k)\big|_{N_{||}=-}\right) \qquad (8$$

where I is the function shown in figure 2. This is a quantity of interest for the current carrying distributions produced in Ohmic slide away and LHCD discharges since, in the energy range of E > 10 keV, $F(+p_{||})$ is small, as the current carriers must move in the $-p_{||}$ direction. The refractive attenuation effects arise through the real part of the dispersion relation Eq. 5 in which $N_{||}$ enters only through $N_{||}^2$ terms. As a result ray bundles differing only in the sign of $N_{||}$ experience equal refractive attenuation. Consequently the ratio of transmitted power of two beams of radiation with opposite launch angle with respect to the normal to $\overline{B}$ can be interpreted as the anti symmetric part of the parallel distribution function through Eq. 8. This ratio is independent of refractive attenuation or any other attenuation even in $N_{||}$. In this experiment the attenuation of two rays with opposite N_{φ}s

are compared since $\bar{B}$ is nearly $B_\varphi \hat{\varphi}$ and $N_{||}$ is nearly N_φ. Ray tracing calculations indicate that the difference in the magnitude of $N_{||}$ for rays of opposite N_φ corresponds to a difference in $p_{||o}$ which is less than the resolution in $p_{||}$ ($\Delta p_{||} \cong .06$) provided $q_a > 7$. this limits the maximum plasma current for which the analysis can be used to approximately 44 kA.

III. Experimental Apparatus

Wave transmission measurements have been performed on the Versator II tokamak with the purpose of determining the parallel distribution of electrons produced in low density ohmic slide away and LHCD plasmas. The Versator II parameters are $B_\varphi = 1.25T$, $\bar{n}_e = 2–20 \times 10^{12} / cm^3$, $I_p = 5–50$ kA, and $T_e = 100–300$ eV. The diagnostic consists of two sets of transmitter and receiver horns, exciting and detecting waves with the polarization perpendicular to the magnetic field ($E \perp B$) at frequencies of 26.5 – 34 GHz ($\omega_{ce}/\omega = 1–1.3$) with transmitted powers of $\simeq$ 1 mW. The horns define the ray paths lying tangential to the constant B_φ surface as shown in figure 3. These rays propagate at angles with respect to the normal to B_φ of $\pm 23^\circ$ with 90% of the power in the X–mode. During an experiment the frequency is swept over the entire range repeatedly with a period of 1 ms. The transmitted power is detected coherently by mixing it with a signal proportional to the launched signal and detecting the low frequency component (homodyne detection). This gives a measure of the amplitude of the transmitted E field multiplied by the sin of the time independent part of its phase. The retention of phase information allows the separation of power transmitted to the receiver in a single pass through the plasma from that which makes multiple passes after being reflected off the vacuum chamber walls. The separation technique is essentially to measure the frequency response of the plasma and vacuum chamber system and use it to calculate the time response to a tone burst pulse, and then to separate the single pass pulse based on its time of flight. To show how this can be done consider the adiabatic limit where the frequency sweep rate of the source is much less than the wave frequency. In this case the electric field seen at the mixer detector at any time during a sweep is equivalent to the electric field due to a steady state sinusoid of frequency equal to the instantaneous

frequency of the source. In this case the received signal during a frequency sweep can be considered as a series of consecutive measurements at different frequencies of the response to a steady state sinusoid. This is given by the

convolution theorem and the definition of the Fourier transform as

$$E(t) = \frac{1}{2\pi}\int_{-\infty}^{+\infty}\left[\int_{-\infty}^{+\infty}\sin(\omega_o t')\, e^{-j\omega t'}\, dt'\right] H(\omega)\, e^{j\omega t}\, d\omega \qquad (9$$

$$= -\frac{j}{2}\left[H(-\omega_o)\, e^{-j\omega_o t} - H(\omega_o)\, e^{j\omega_o t}\right]$$

where $H(\omega)$ is the Fourier transform of the system impulse response, $h(t)$.

$$H(\omega) \equiv \int_{-\infty}^{+\infty} h(t)\, e^{-j\omega t}\, dt \qquad (10$$

The mixer then multiplies this signal with a reference signal and averages over many periods to give a voltage;

$$V(\omega_o) = \langle E(t)\sin(\omega_o t)\rangle \qquad (11$$

$$= \frac{1}{4}\left(H(-\omega_o) + H(\omega_o)\right)$$

This voltage is recorded continuously as a function of ω_o over some range $\omega_1 \pm \Delta\omega$. Recognizing that the measured voltage is essentially the Fourier transform of the system's impulse response allows calculation of the impulse response by inverting the transform.

$$V'(t') \equiv \frac{1}{2\pi}\int_{\omega_1-\Delta\omega}^{\omega_1+\Delta\omega} V(\omega_o)\, e^{j\omega_o t'}\, d\omega_o \qquad (12$$

Inserting $V(\omega_o)$ and the definition of the impulse response $h(t)$ gives, for transit times $t' > 2\pi/\Delta\omega$;

$$V'(t') \simeq \frac{1}{4\pi}\int_{-\infty}^{+\infty} h(t'-t)\,\frac{\sin(\Delta\omega t)}{t}\, e^{-j\omega_1 t}\, dt \qquad (13$$

This is recognized as the impulse response of the system to a tone burst with frequency ω_1 and a modulation envelope of $\sin(\Delta\omega t)/t$. The $|V'(t)|$ calculated numerically from the $V(t)$ measured with an empty vacuum chamber and with a plasma present and is plotted for ω_1 = 28 GHz, ω_{ce} = 35 Ghz, and $\Delta\omega$ = 1.33 GHz in figure 4. Here the first group of peaks between t = 10–15 ns corresponds to the pulse response of a single receiving horn. The first peak is caused by radiation making a single

pass through the vacuum chamber. Later peaks are separated by ~ 2 ns corresponding to the time delay in vacuum for multiple bounces off the top and bottom of the vacuum chamber. In order to allow simultaneous measurements of transmission on two rays with the same detector, the signal from the second receiver horn has been delayed in time by ~ 25 ns and sent to the same mixer. This produces the second group of peaks between t = 35–40 ns. The amplitude of the initial peak in each group is normalized to what it is in the vacuum case to give the transmission coefficient for wave amplitude with no need for absolute calibration. This is done at five different frequencies each millisecond, providing a measure of the transmission coefficient vs. ω_{ce}/ω. The rejection of the unwanted multi–pass peaks was found to be ≥ 20 dB in the empty vacuum chamber. This has allowed operation of the diagnostic with no microwave absorbing material to disturb the plasma or vacuum system.

IV. Experimental Results

Results have been obtained for the time response of the transmission coefficient and distribution function both in low density Ohmic discharges where the electric field produces energetic slide away electrons, and during lower hybrid current drive (LHCD) where quasi linear diffusion sustains the energetic particles. The time history of plasma parameters for the Ohmic discharges is shown in figure 5. The Electron Cyclotron Transmission (ECT) data was collected during a 7 ms period at the initiation of the current pulse. The frequency was swept once per millisecond and the transmission was measured at 5 frequencies at each of 7 time steps. The results are shown in Fig. 6 with error bars representing the standard deviation of four discharges. The first time step shows substantial and nearly equal attenuation on both ray paths, consistent with attenuation mechanisms, such as refraction, that are even in $N_{||}$ and hence launch angle. Later in time the attenuation on the ray path which is resonant with the energetic electron tail increased, indicating the presence of current carrying electrons with momentum opposite to the direction of positive current flow. The second time step shows the asymmetry in transmission primarily in the lowest two ω_{ce}/ω cases corresponding to

electrons appearing first at low energy. At later times the transmission asymmetry was also present at higher values of ω_{ce}/ω corresponding to increasing electron energy with time. This time dependence is similar to the ~ 2 ms rise time of the emission of radiation at the second harmonic of the cyclotron frequency perpendicular to B in the horizontal plane (2Fce in fig. 5). For the optically thin Versator II plasmas this emission is an indication of suprathermal electrons. The last frame shows the asymmetry in transmission for t ~ 15 ms for a discharge where the direction of current flow was reversed, and shows a clear reversal of the asymmetry. Finally the attenuation of the ray which was not resonant with the current carrying electrons is averaged over all time steps and shown in figure 7 compared with theoretical calculations of refractive attenuation for this case that was described in Section II. The measurements indicate somewhat greater nonresonant attenuation than is predicted by the ray tracing calculation of refraction. This could be explained by other processes not included in the ray tracing calculation such as scattering from plasma turbulence, cyclotron absorption on a symmetric distribution of energetic particles, or variations of the density profile from the parabolic model assumed.

The time dependence of the distribution function deduced from the asymmetric part of the transmission via the method of section II is shown in figure 8 along with an analytic calculation for the shape of the distribution of runaway electrons when confinement is ideal [12]. The parameters for the calculation were V_{loop}= .58 V, Z_i= 2, n_e= $2x10^{12}/cm^3$. The time dependence of the distribution shows particles progressing from low energy to high energy in response to the applied electric field. In particular the distribution function at t = 1 ms is essentially zero in all energy bins, while the following time steps show electrons appearing first at low energy and then at higher energies. A steady state was reached after 4 ms, where the velocity moment of the measured distribution function indicates that 42 % of the total plasma current is carried by particles in the energy range of the measurement. The $T_{||}$ determined from a best fit to a maxwellian is 45 keV which is not quite as high as the prediction shown in figure 8. It is also noted that the highest ω_{ce}/ω (highest energy) point

shows a small asymmetry at t = 1 ms, when there should be no energetic particles present. That the asymmetry in the highest ω_{ce}/ω measurements is caused by a small asymmetry in the measurement system is indicated by the fact the asymmetry reverses when the current reverses. In fact, accounting for asymmetries in the instrument by normalizing all measured asymmetries in transmission to the earliest in time measurement brings the distribution measured with the current forward and reversed into closest agreement. This leads to the correction shown in the 5 to 7 ms distribution shown in figure 8. Other measurements made out to t = 13 ms showed little difference from the distributions measured for t= 4–7 ms. Measurements of the hard x–ray spectrum between 20 keV and 200 keV show that the count rate decreases by a factor of 100 from 20 to 160 keV ($T_{hx} \sim 30$ keV) indicating that few particles were present above the 200 keV energy cutoff assumed in the analysis of $F(p_{||})$. However measurements of hard x–rays in the range 20 keV – 200 keV provide little additional information about the particles in the range of the cyclotron transmission diagnostic (5 keV – 50 keV) due to the fact that they represent an integral over momentum space which includes particles above 50 keV. A calculation of the $T_{\perp}$ for this case is presented in Ref. [12] and gives $T_{\perp}$ = 2 to 8.5 keV in this energy range which supports the low $T_{\perp}$ assumption in the above analysis

Measurements have also been made in discharges where the current was sustained by lower hybrid current drive and the single turn loop voltage was approximately zero. The time history of the plasma parameters are shown in Figure 9. The R.F. system operated at a frequency of 2.45 GHz and launched lower–hybrid waves by means of a four waveguide antenna. This system is described in Ref. [13]. The primary difference between the initial inductive phase of these discharges and the previous ones is that in the former the initial density was much higher and the loop voltage was somewhat lower. These changes were made in order to reduce the slide away population produced in the start up phase, so as to minimize the suprathermal population before the R. F. drive was initiated. The Ohmic heating transformer was open circuited at t=5 ms and the current was allowed to inductively decay. The R. F. power was turned on at 16 ms which forces the plasma loop voltage to

near zero by ~ 18 ms. The flat top current was then sustained at a level of 18 kA, Fig. 9. The electron cyclotron transmission measurement was started 1 ms before the beginning of the R. F. pulse and continued 6 ms into the flat top region. In order to reduce statistical variations the measured distributions have been averaged over the first and second, third through fifth, and sixth and seventh time steps, as well as over four identical discharges. The results are shown in figure 10 with error bars representing the standard deviation of four discharges. Fast electrons were seen to be sustained during the R. F. pulse as expected during steady state R. F. current drive. The slope of the distribution decreased slightly as the loop voltage fell, reaching an equilibrium in $\lesssim$ 2.5 ms. The rise time of the radiation at the second harmonic of ω_{ce} was also ~ 2.5 ms. From the measured $F(p_{||})$ the equilibrium current carried by the particles in this energy range is calculated to be .7 I_{total}. These measurements indicate that the suprathermal distribution was being sustained by the lower hybrid waves in the absence of electric fields in qualitative agreement with the theory of LHCD [14]. A calculation of the $T_{\perp}$ for this case is presented in Ref.[15] where the distribution is assumed flat between zero and some cutoff energy. Using a cutoff energy of 50 keV, V_{loop}=0, and other parameters the same as for the inductive case, this calculation gives $T_{\perp} \leq 7.5$ keV, justifying the analysis for determining $F(p_{||})$.

V. Conclusions

It has been shown theoretically that the measurement of absorption rate at and below the electron cyclotron frequency can give a direct measure of the perpendicularly averaged current carrying distribution function $F(p_{||})$, if the $T_{\perp}$ is sufficiently low ($T_{\perp} \lesssim 15$ keV) and $T_{||}$ is sufficiently high ($T_{||} \gtrsim E_{||}$). The effect of refractive attenuation can be removed because of its symmetry in $N_{||}$ by making measurements along two ray paths with equal and opposite $N_{||}$. This is achieved by launching radiation along paths oppositely directed in φ which for sufficiently low current ($q_a > 7$) provides nearly opposite ($N_{||}$). A technique has been demonstrated to measure the single pass absorption rate even in the presence of reflecting chamber walls. The results show the non–resonant attenuation of

radiation in this range to be somewhat greater than that which can be explained by refraction alone. The additional resonant part of the attenuation caused by absorption by energetic electrons is consistent in frequency dependence, time dependence, and amplitude with measurements of cyclotron emission and total plasma current. The measured distribution function $F(p_{||})$ during inductive drive shows a large parallel temperature, but one that is lower than is predicted for Coulomb scattering alone. During the R. F. current drive, $F(p_{||})$ is found to flatten and increase above the level established during the inductive phase of the discharge. This technique provides a new measure of the suprathermal distribution of electrons in tokamak plasmas.

Acknowledgements

The authors would like to thank A. H. Kritz, and G. R. Smith for their assistance in running the ray tracing codes, and K.–I. Chen for operation of the Versator machine, and acknowledge the able technical assistance of Edward Fitzgerald and John Nickerson. One of the authors (R.K.K.) is happy to acknowledge useful conversations with I. Fidone and R. L. Meyer. This work was supported by U.S. Department of Energy contract # DE–AC02–78ET–51013. R. K. K. was supported by a TRW Inc. doctoral fellowship.

References

1. M. Bornatici, R. Cano, O. De Barbieri, and F. Engelmann, Nucl. Fusion 23, 1153 (1983).

2. A. C. Riviere, Plasma Phys. and Contr. Fusion, 28, 1263 (1986).

3. A. Ando, K. Ogura, H. Tanaka, M. Iida, S. Ide, K. Oho, S. Ozaki, T. Cho, T. Maekawa, Y. Teramichi, and S. Tanaka, Phys. Rev. Lett. 56, 2180 (1986).

4. A. Ando, K. Ogura, H. Tanaka, M. Iida, S. Ide, T. Maekawa, Y. Teramichi, and S. Tanaka, Nucl. Fusion 26, 107 (1986).

5. I. H. Hutchinson, and K. Kato, Nucl. Fusion, 26, 179 (1986).

6. K. Kato, and I. H. Hutchinson, Phys. Rev. Lett. 56, 340 (1986).

7. E. Mazzucato, P. Efthimion and I. Fidone, Nucl. Fusion 25, 1681 (1985).

8. I. Fidone, G. Granata, and R. L. Meyer, Phys. Fluids 25, 2249 (1982).

9. G. Giruzzi, I. Fidone, G. Granata, and R. L. Meyer, Phys. Fluids 27, 1704 (1984).

10. I. Fidone, G. Giruzzi, G. Granata, and R. L. Meyer Phys. Fluids 27, 661 (1984).

11. G. R. Smith, Lawrence Livermore Lab., private communication 1988.

12. V. Fuchs, R. A. Cairns, C. N. Lashmore–Davies, M. M. Shoucri, Phys. Fluids, 29, 2931 (1986).

13. M. J. Mayberry, M. Porkolab, K.–I. Chen, A. S. Fisher, D. Griffin, R. D. Kaplan, S. C. Luckhardt, J. Ramos, and R. Rohatgi, Phys. Rev. Lett. 55, 829 (1985).

14. Nathaniel J. Fisch, Rev. Mod. Phys. 59, 1, 175 (1987)

15. V. Fuchs, R. A. Cairns, M. M. Shoucri, K. Hizanidis and A. Bers, Phys. Fluids 28, 3619 (1985).

Figure Captions

1. Resonance contour in momentum space for waves with $N_{||} = 0$ and 0.4 for frequencies just below the cyclotron fundamental.

2. Numerical calculation of the imaginary part of N due to suprathermal electrons for $N_{||} = 0.4$ in the limit $k_{\perp} \rho_e << 1$. N_i is averaged over parabolic density and current profiles for $F(p_{||}) = 10^{11}/cm^3$, $T_{\perp} = 1$ keV, for peak densities $n_e = 2$ to 10 x 10^{12} / cm^3.

3. Experimental configuration of the two ray measurement showing the mixer for signal detection and delay line.

4. System fast time response calculated from measured data, with and without plasma for $\omega_{ce}/\omega = 1.2$, $\bar{n}_e = 2 \times 10^{12} / cm^3$. The peaks between 10 and 20 ns are caused by the initial ray and its reflections from the vacuum vessel. The peaks between 35 and 45 ns are caused by the delayed ray.

5. Plasma time history for Ohmic case showing measurement period for the transmission diagnostic (ECT).

6. Time history of the received electric field during the Ohmic discharge showing similar transmission characteristics for both resonant and non–resonant rays at t = 1 ms, and an asymmetric reduction in transmission progressing from low ω_{ce}/ω to high ω_{ce}/ω in time. Also shown is a late in time measurement with similar conditions but with the current reversed,

showing reversal of the attenuation asymmetry.

7. Transmission of the non–resonant ray in the Ohmic case, compared with refractive attenuation calculated by the toroidal ray tracing code.

8. The asymmetric part of the momentum distribution function ($F_a(p_{||}) \equiv 1/2(F(p_{||}) - F(-p_{||}))$) vs. parallel energy deduced from the asymmetry in transmission measured in the Ohmic case at different times, is compared with theory for the equilibrium distribution function for ideal confinement from Ref [12].

9. Plasma time history for the LHCD case showing measurement time period for the transmission diagnostic (ECT) and forward R. F. power.

10. The asymmetric part of the momentum distribution vs. parallel energy deduced from the asymmetry in the transmission measured during the initiation of lower hybrid current drive.

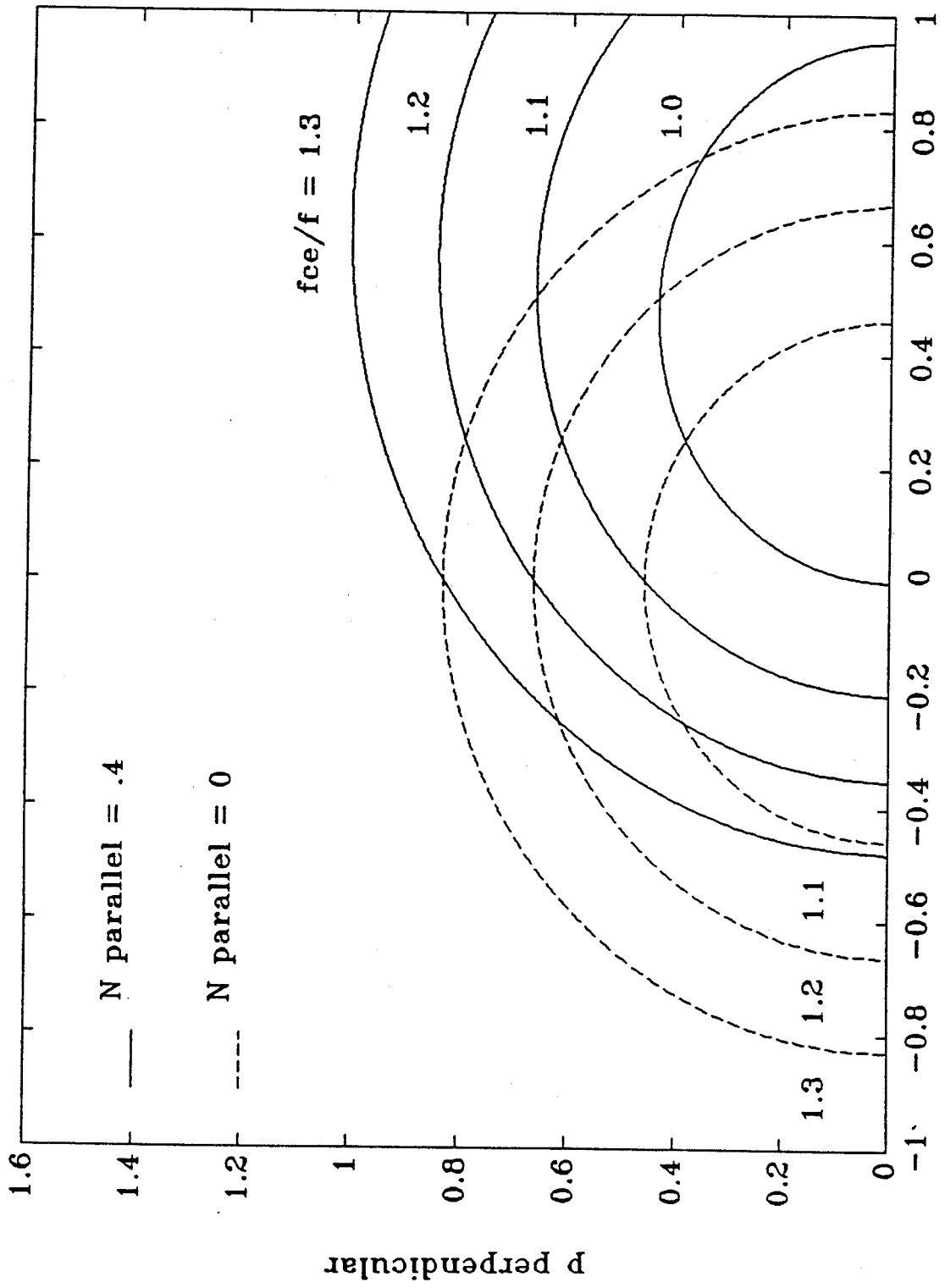
N parallel = .4
N parallel = 0
fce/f = 1.3
1.2
1.1
1.0
1.3
1.2
1.1
p perpendicular
p parallel
1.6
1.4
1.2
1
0.8
0.6
0.4
0.2
0
-1
-0.8
-0.6
-0.4
-0.2
0
0.2
0.4
0.6
0.8
1

figure 1.

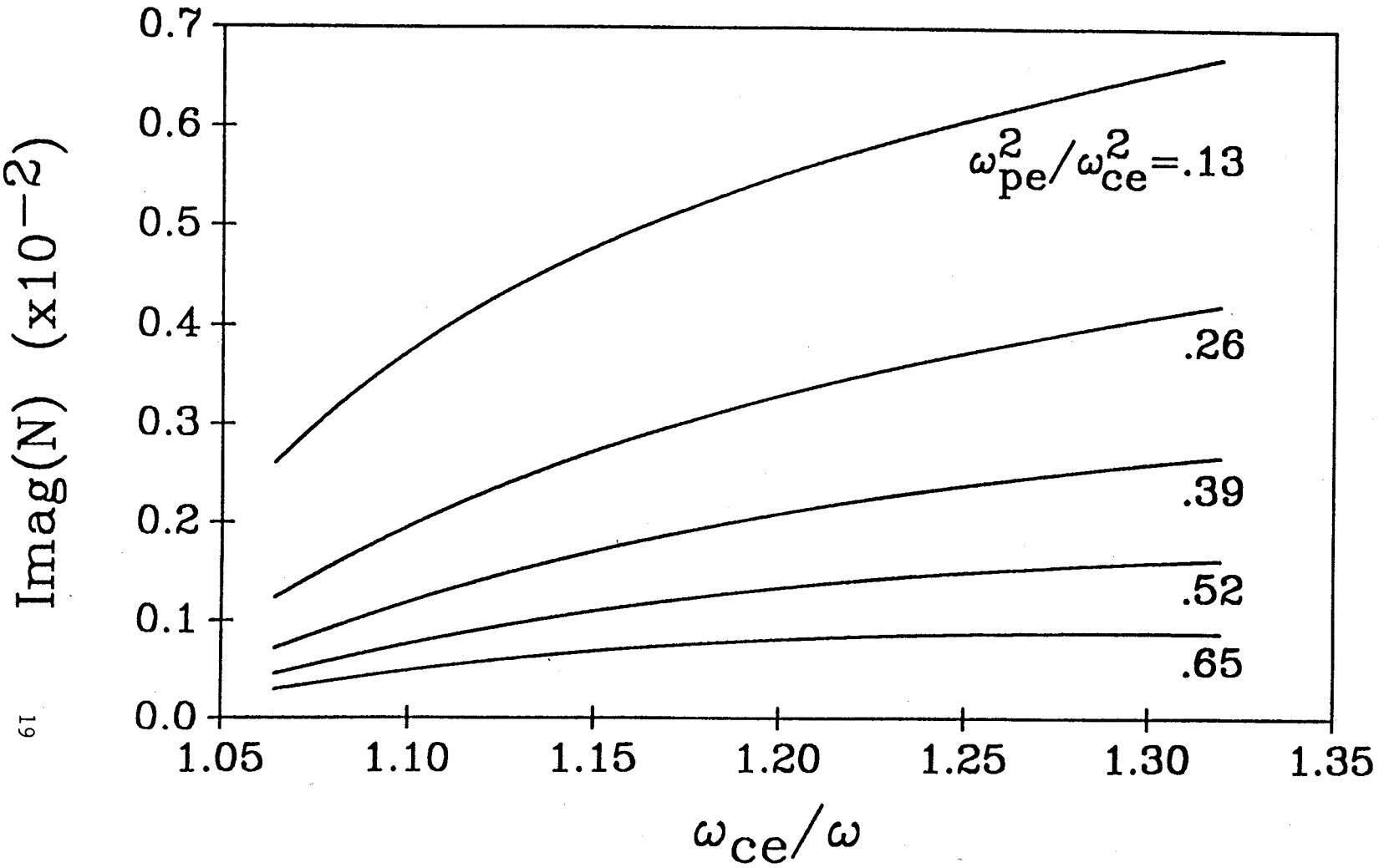
0.7
0.6
0.5
0.4
0.3
0.2
0.1
0.0
Imag(N) (x10⁻²)
$\omega_{pe}^2/\omega_{ce}^2$=.13
.26
.39
.52
.65
1.05
1.10
1.15
1.20
1.25
1.30
1.35
ω_{ce}/ω

figure 2.

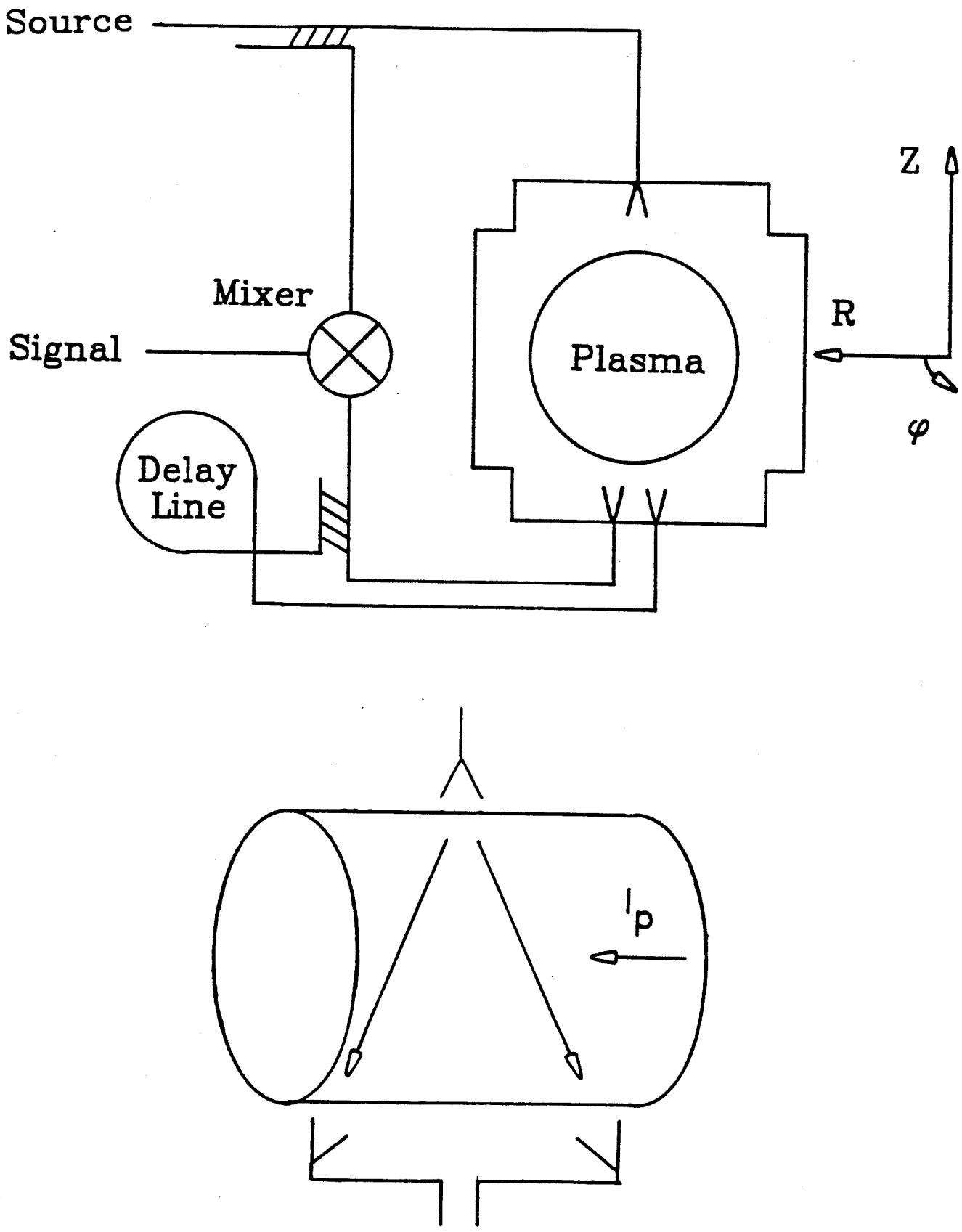

figure 3.

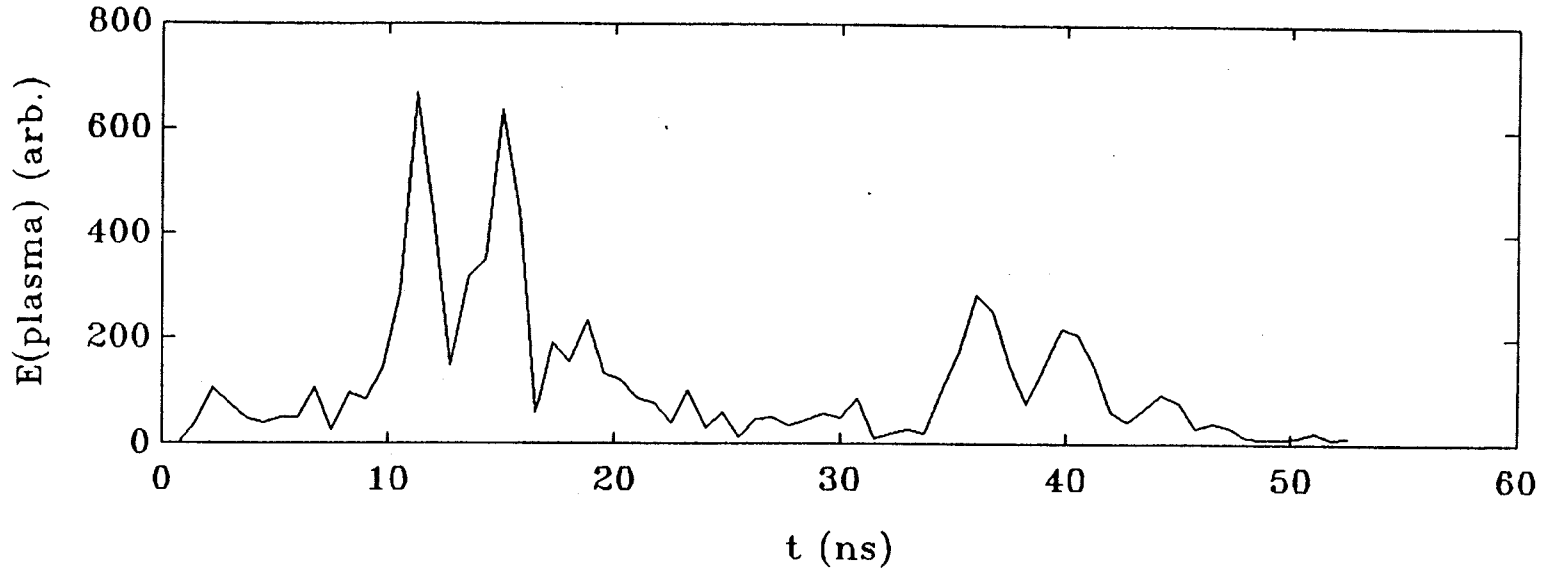
800
600
400
200
0
E(plasma) (arb.)
0
10
20
30
40
50
60
t (ns)

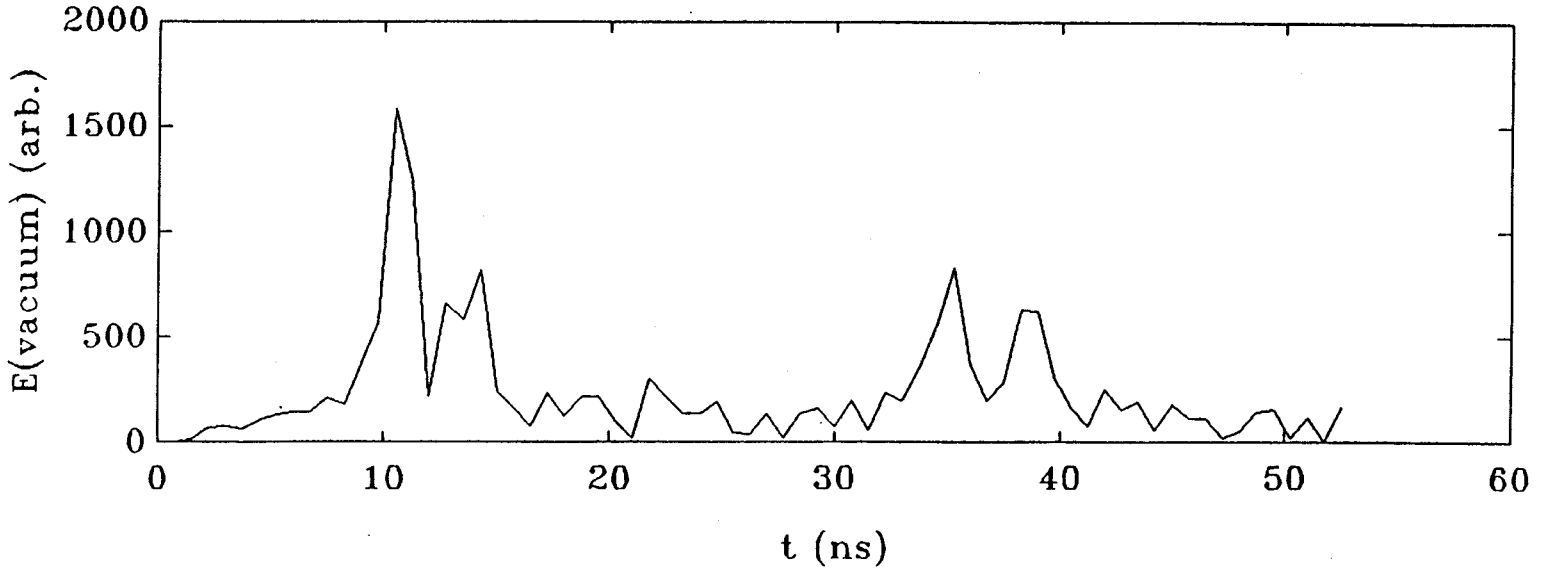
2000
1500
1000
500
0
E(vacuum) (arb.)
0
10
20
30
40
50
60
t (ns)

figure 4.

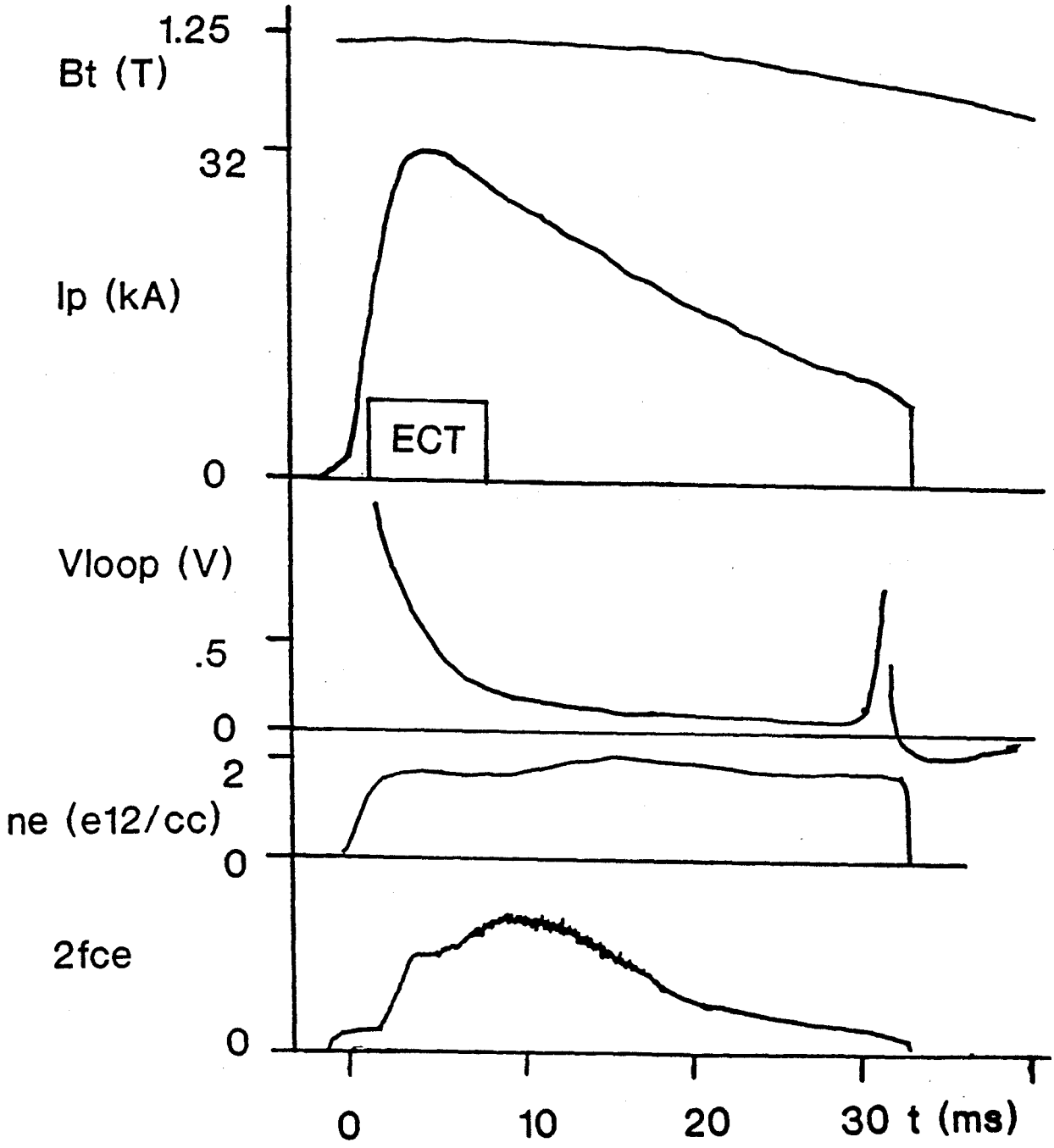

figure 5.

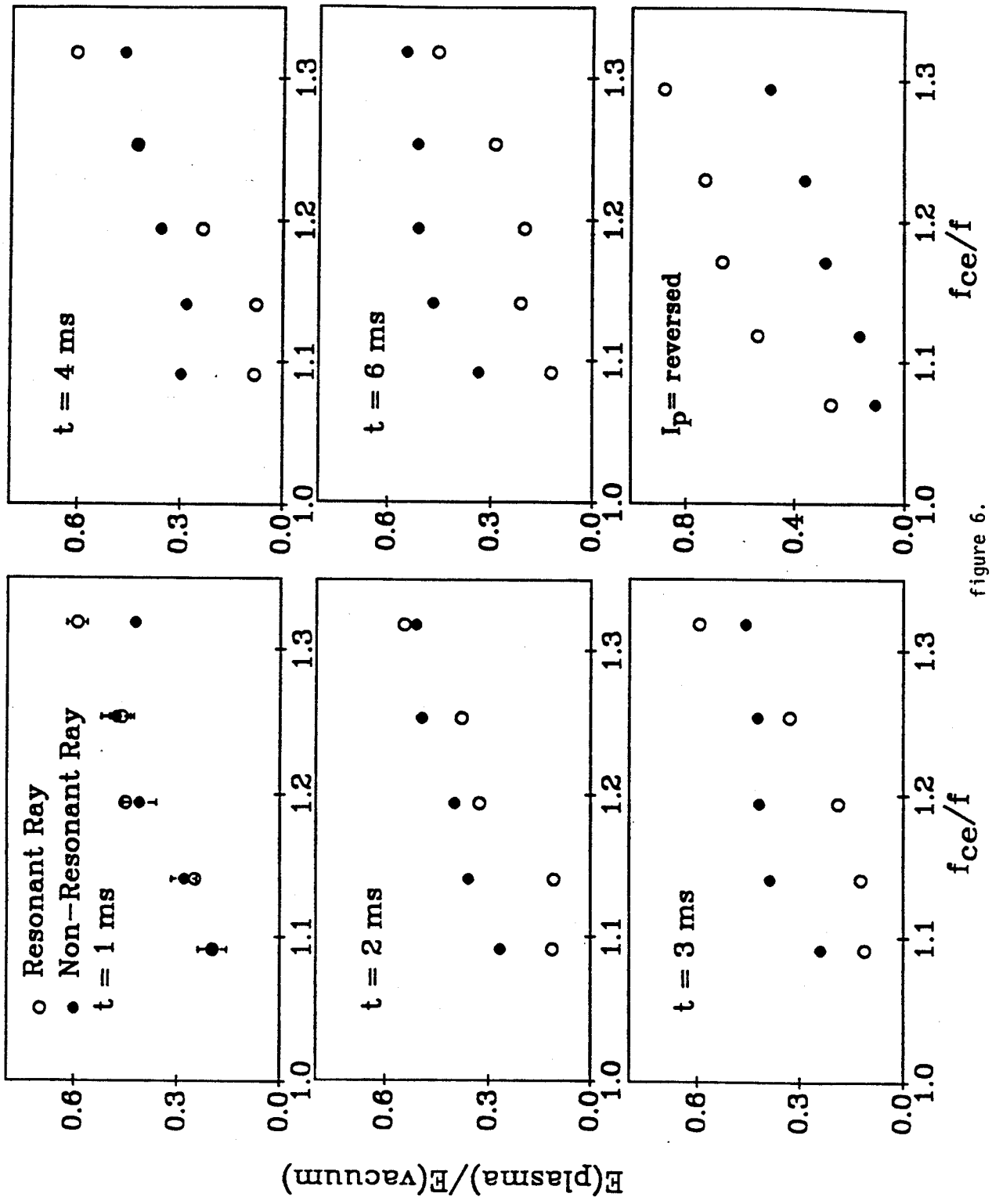
o Resonant Ray
• Non-Resonant Ray
t = 1 ms
t = 2 ms
t = 3 ms
t = 4 ms
t = 6 ms
Ip= reversed
E(plasma)/E(vacuum)
fce/f
0.0
0.3
0.6
0.4
0.8
1.0
1.1
1.2
1.3

figure 6.

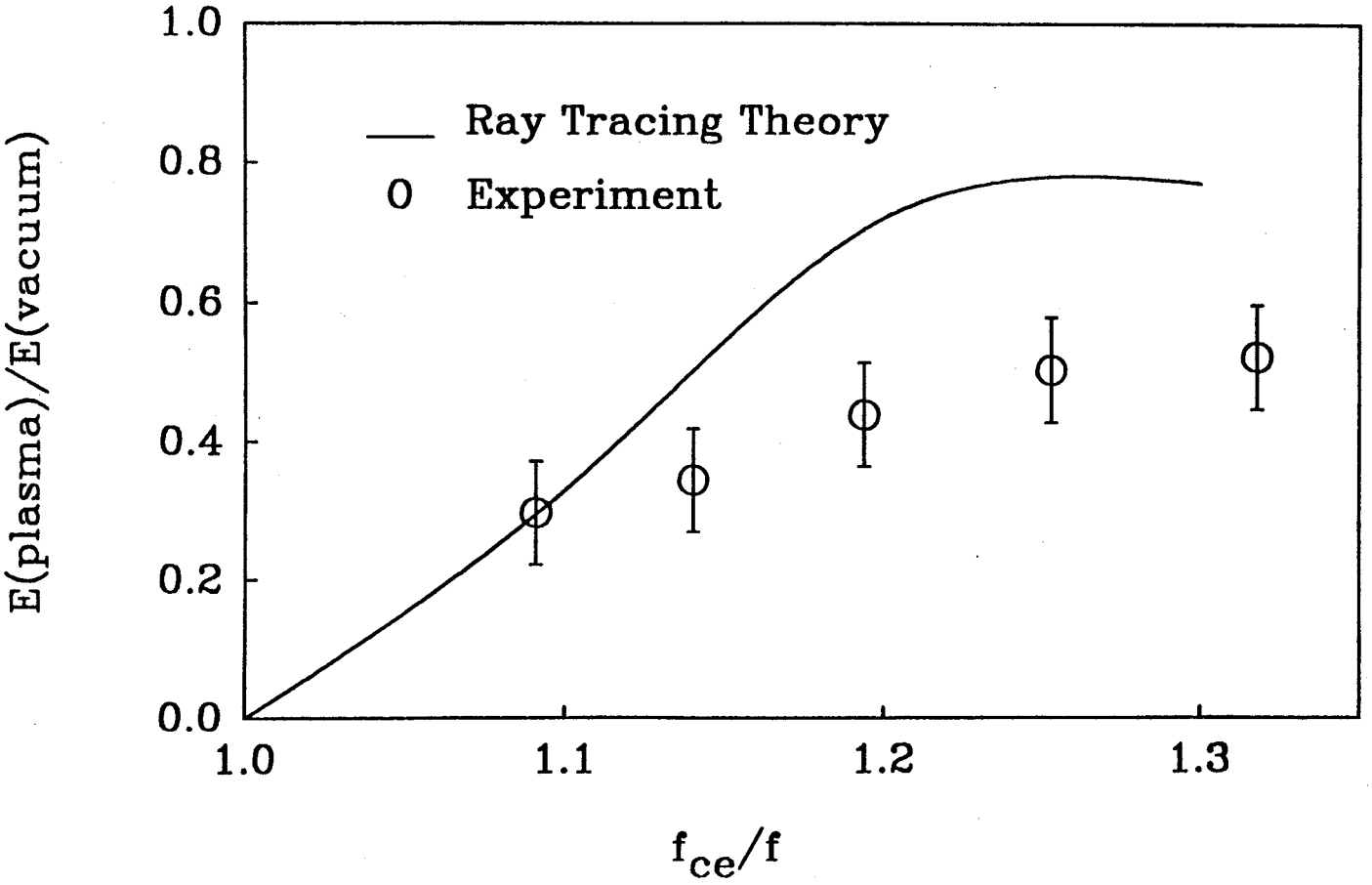
1.0
0.8
0.6
0.4
0.2
0.0
1.0
1.1
1.2
1.3
Ray Tracing Theory
Experiment
E(plasma)/E(vacuum)
f_{ce}/f

figure 7.

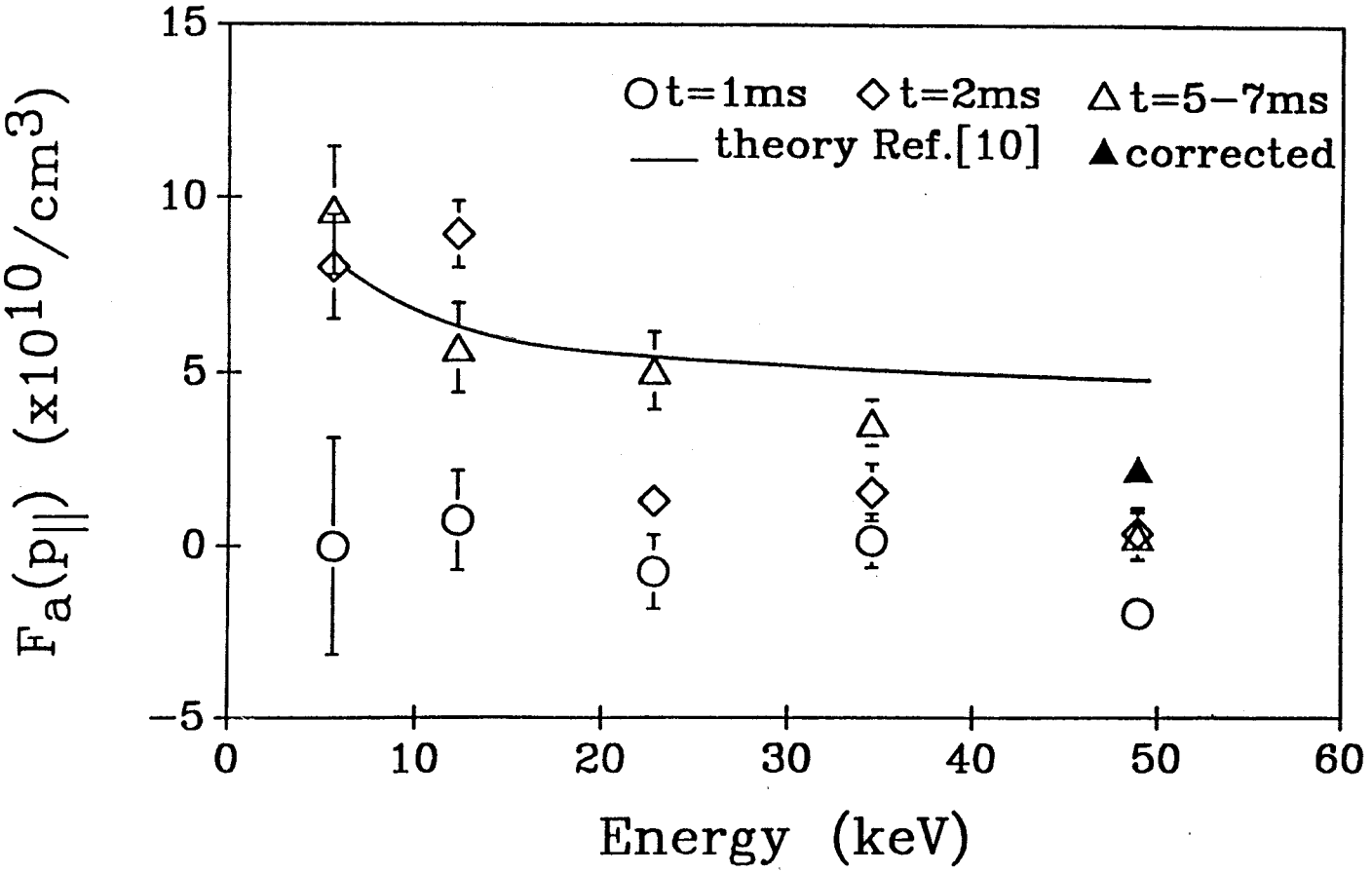
15
10
5
0
−5
0
10
20
30
40
50
60
Energy (keV)
$F_a(p_\parallel)$ (x1010/cm3)
O t=1ms
◇ t=2ms
△ t=5−7ms
___ theory Ref.[10]
▲ corrected

figure 8.

figure 9.

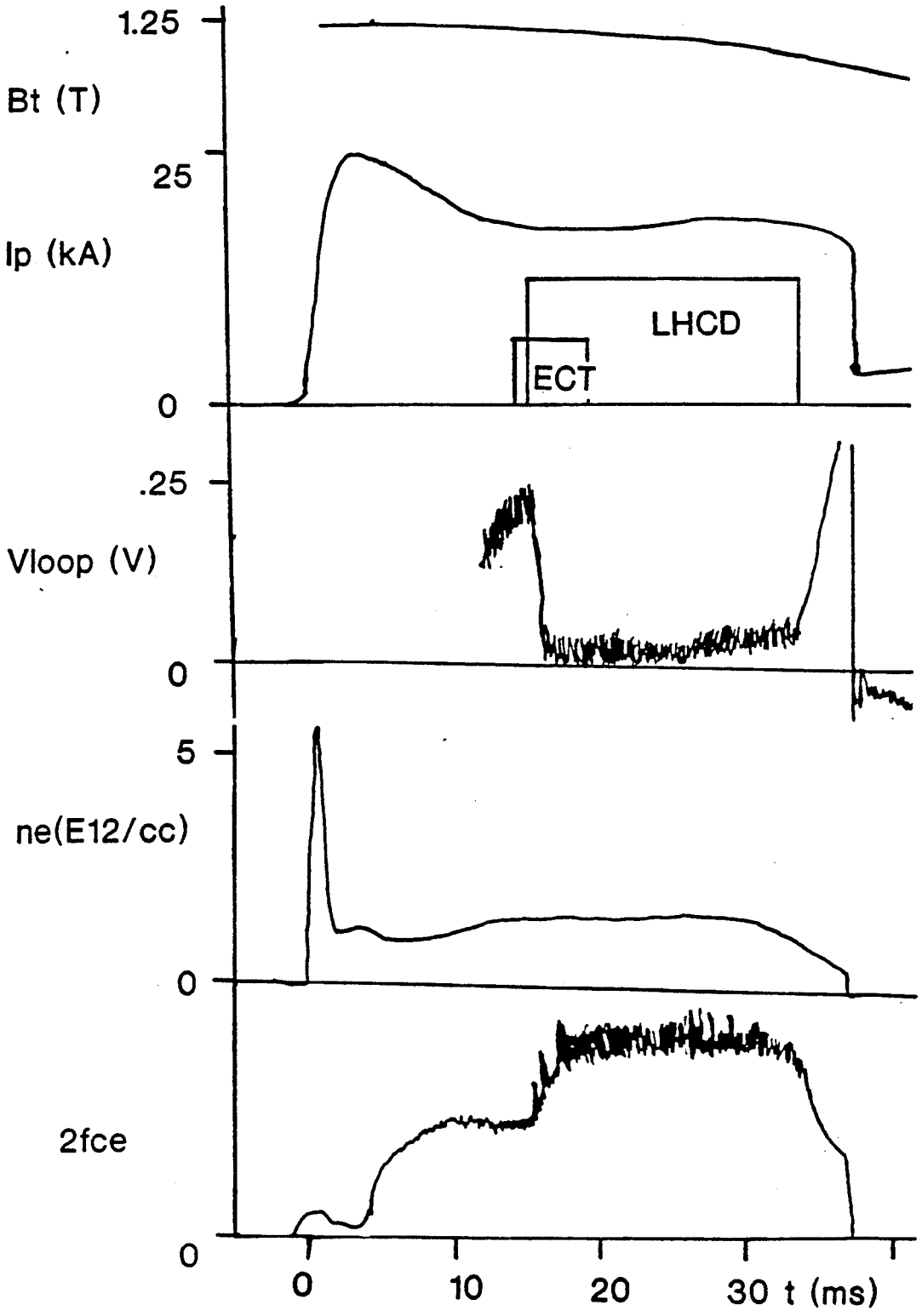
1.25
Bt (T)
25
Ip (kA)
0
LHCD
ECT
.25
Vloop (V)
0
5
ne(E12/cc)
0
2fce
0
0
10
20
30 t (ms)

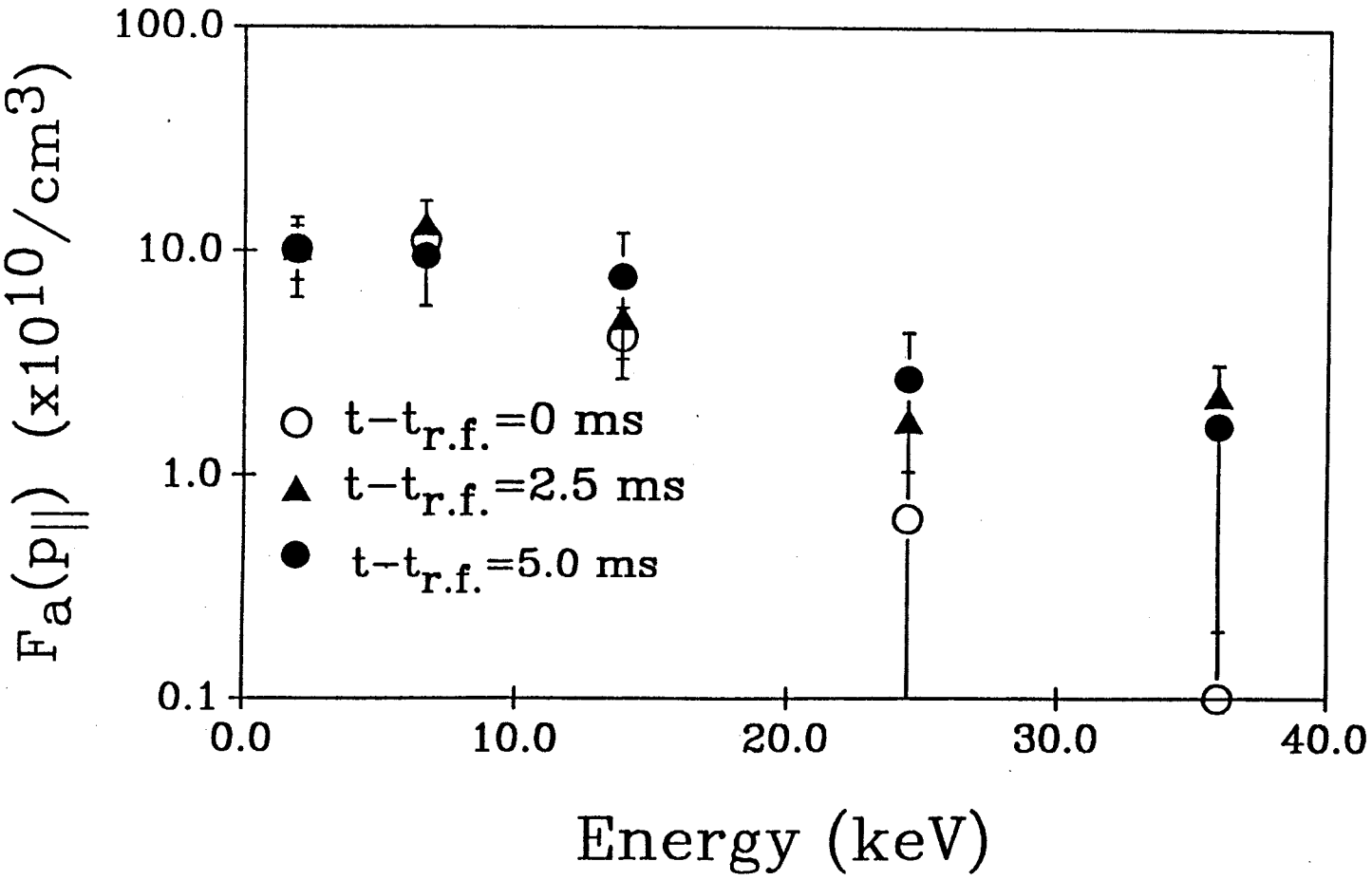
100.0
10.0
1.0
0.1
0.0
10.0
20.0
30.0
40.0
$F_a(p_{||})$ (x10^{10}/cm^3)
Energy (keV)
$t-t_{r.f.}$=0 ms
$t-t_{r.f.}$=2.5 ms
$t-t_{r.f.}$=5.0 ms

figure 10.